https://doi.org/10.1093/plphys/kiad652 PLANT PHYSIOLOGY 2023: 00: 1–9

Plant Physiology®

Research Report

Genetic dissection of *cis*-regulatory control of *ZmWUSCHEL1* expression by type B RESPONSE REGULATORS

Zongliang Chen,[1] **Liz Cortes**[1] **and Andrea Gallavotti**[1,2,*]

1 Waksman Institute of Microbiology, Rutgers University, Piscataway, NJ 08854-8020, USA
2 Department of Plant Biology, Rutgers University, New Brunswick, NJ 08901, USA

*Author for correspondence: agallavotti@waksman.rutgers.edu
The author responsible for distribution of materials integral to the findings presented in this article in accordance with the policy described in the Instructions for Authors (https://academic.oup.com/plphys/pages/General-Instructions) is Andrea Gallavotti.

Abstract

Mutations in *cis*-regulatory regions play an important role in the domestication and improvement of crops by altering gene expression. However, assessing the in vivo impact of *cis*-regulatory elements (CREs) on transcriptional regulation and phenotypic outcomes remains challenging. Previously, we showed that the dominant *Barren inflorescence3* (*Bif3*) mutant of maize (*Zea mays*) contains a duplicated copy of the homeobox transcription factor gene *ZmWUSCHEL1* (*ZmWUS1*), named *ZmWUS1-B*. *ZmWUS1-B* is controlled by a spontaneously generated novel promoter region that dramatically increases its expression and alters patterning and development of young ears. Overexpression of *ZmWUS1-B* is caused by a unique enhancer region containing multimerized binding sites for type B RESPONSE REGULATORs (RRs), key transcription factors in cytokinin signaling. To better understand how the enhancer increases the expression of *ZmWUS1* in vivo, we specifically targeted the *ZmWUS1-B* enhancer region by CRISPR-Cas9-mediated editing. A series of deletion events with different numbers of type B RR DNA binding motifs (AGATAT) enabled us to determine how the number of AGATAT motifs impacts in vivo expression of *ZmWUS1-B* and consequently ear development. In combination with dual-luciferase assays in maize protoplasts, our analysis reveals that AGATAT motifs have an additive effect on *ZmWUS1-B* expression, while the distance separating AGATAT motifs does not appear to have a meaningful impact, indicating that the enhancer activity derives from the sum of individual CREs. These results also suggest that in maize inflorescence development, there is a threshold of buffering capacity for *ZmWUS1* overexpression.

Introduction

The Arabidopsis (*Arabidopsis thaliana*) homeobox-encoding gene *WUSCHEL* (*WUS*) plays a crucial role in controlling stem cell populations in a specific functional domain of the shoot apical meristem called the organizing center and is regulated by a negative feedback loop called the CLAVATA/WUS pathway (Kitagawa and Jackson 2019). WUS can function both as an activator and repressor of transcription (Ikeda et al. 2009). Notably, in the meristem central zone, WUS positively regulates *CLAVATA3* (*CLV3*) expression, which encodes a short peptide that in turn, together with its antagonistic peptide CLE40 (CLAVATA3/EMBRYO SURROUNDING REGION 40), restricts *WUS* expression to the organizing center domain to buffer and maintains a stable population of stem cells (Ikeda et al. 2009; Perales et al. 2016; Plong et al. 2021; Schlegel et al. 2021). In Arabidopsis, it was shown that the shoot apical meristem can sustain up to 10-fold upregulation

Received September 13, 2023. Accepted November 06, 2023. Advance access publication December 7, 2023

Open Access

of *CLV3* without affecting meristem development (Müller et al. 2006). On the other hand, CRISPR-Cas9 editing of the *ZmCLE7* and *ZmFCP1* promoters, 2 maize (*Zea mays*) *CLV3* homologs that negatively regulate inflorescence meristem size and ear row number, showed that even limited expression perturbations (45% to 69% reduced expression) increased inflorescence meristem size and enhanced grain yield–related traits (Liu et al. 2021). This indicates that the buffering capacity of the CLV-WUS pathway varies among different plant species.

Recently, it was revealed that type B ARABIDOPSIS RESPONSE REGULATORs (ARRs) directly bind to the *Arabidopsis WUS* promoter and activate *WUS* expression (Zhang et al. 2017; Zubo et al. 2017; Xie et al. 2018). The binding of type B ARRs occurs to a single motif in the *WUS* promoter. The AGATAT-binding site for type B ARRs, including ARR1, ARR10, and ARR12, found in the *Arabidopsis WUS* was only evident when *Arabidopsis* plants were subjected to cytokinin treatments (Zubo et al. 2017; Xie et al. 2018) or when *ARR1* and *ARR2* were constitutively overexpressed (Zhang et al. 2017). In tomato (*Solanum lycopersicon*), a majority of CRISPR-Cas9-mediated deletions in a 2.5 kb region of the *SlWUS* promoter failed to alter fruit development suggesting that the core elements of *WUS* transcriptional regulation reside in a small region containing 1 AGATAT motif proximal to the transcription start site or that the promoter of *SlWUS* is very tolerant to perturbations (Wang et al. 2021).

The maize *ZmWUS1* gene is a coortholog of *Arabidopsis WUS* and plays a conserved role in controlling stem cell populations in inflorescence meristems (Nardmann and Werr 2006; Chen et al. 2021). The maize *Barren inflorescence3* (*Bif3*) mutant, harboring a duplicated copy of *ZmWUS1*, named *ZmWUS1-B*, shows overproduction of stem cells in inflorescence meristems and is caused by the increased expression of *ZmWUS1-B* (Chen et al. 2021). We previously showed that the increased activity of the *ZmWUS1-B* promoter is due to the presence of a 119 bp enhancer region at the 5′ duplication junction site. Enhancers are collections of *cis*-regulatory elements (CREs) that confer tissue-specific gene expression by the interaction of transcription factors (TFs) with specific DNA sequences. This region carries 3 additional AGATAT motifs, rather than a single motif found in the wild-type (WT) *ZmWUS1* promoter (Chen et al. 2021). However, how these additional AGATAT *cis*-regulatory motifs function to regulate in vivo *ZmWUS1* expression is unclear.

Results and discussion

Given the presence of AGATAT motifs in the promoters of *WUS* orthologs in Arabidopsis, tomato, and maize, we sought to understand the variability of this feature across plant species. In both monocot and dicot species, a single AGATAT motif is normally present in a similar position in the proximal promoter region, with the notable exception of coffee (*Coffea arabica*) where the motif is present in the first intron (Fig. 1 and Supplemental Fig. S1). We subsequently asked whether the WT promoter of the *ZmWUS1* gene encompassed regions of evolutionary conservation within monocots. We retrieved sequences 5 kb upstream and 2 kb downstream of the *WUS* coding sequence for several monocot species and found conserved regions not only within the gene body, as expected, but also in the proximal promoter, including an 84 bp stretch of noncoding sequence conserved across the Panicoideae subfamily (Fig. 1A). An additional assessment of the evolution of noncoding sequences using a model-based approach, which compares the substitution rate in regions of interest to a neutral model, produced similar outcomes (Fig. 1B). However, this approach also uncovered a distal promoter region (−1,000 to −5,000; Fig. 1A) of increased substitutions in monocots, suggesting that the regulation of *ZmWUS1* by the proximal promoter region is subject to positive selection. Interestingly, the 84 bp conserved noncoding sequence also overlapped with an accessible chromatin region, as determined by both Assay for Transposase-Accessible Chromatin using Sequencing (ATAC-seq) (Hufford et al. 2021) and MNase-defined cistrome-Occupancy Analysis (MOA-seq) (Savadel et al. 2021) (Fig. 1C). Part of this region (a 69 bp fragment carrying a single type B RR motif) was duplicated in the 119 bp *ZmWUS1-B* enhancer, which together with 2 AGATAT motifs flanking the 69 bp fragment, resulted in a total of 3 additional type B RR motifs in the *ZmWUS1-B* promoter region (Fig. 1D) (Chen et al. 2021).

To uncover the function of both the conserved noncoding sequence and the type B RR binding sites, we used CRISPR-Cas9 to edit the 119 bp *ZmWUS1-B* enhancer. Two single-guide RNAs (sgRNAs) were designed to target its flanking regions: sgRNA1 was located at the 3′ junction region of the enhancer insertion site and endogenous *ZmWUS1-B* promoter, while sgRNA2 was located 21 bp upstream of the enhancer region (Fig. 2A). The construct was introduced into the B104 inbred line by *Agrobacterium tumefaciens*–mediated transformation, and then, T0 plants carrying the transfer DNA (T-DNA) were crossed to *Bif3* mutants in the A619 inbred background which was previously shown to be more sensitive to *ZmWUS1* overexpression (Chen et al. 2021). The resulting T1 plants were first genotyped for the *Bif3* mutation and subsequently for editing in the enhancer region. Five enhancer-edited alleles were isolated (Supplemental Fig. S2), and they were named *Bif3-Δ113*, *Bif3-Δ33*, *Bif3-Δ15*, *Bif3-Δ4*, and *Bif3-Δ1* according to the sizes of DNA deletions. Plants carrying each allele were backcrossed 3 times to A619 to allow phenotypic comparisons with the original *Bif3* mutant which showed a dominant and severe effect on ear development (Chen et al. 2021). Throughout this process, we also segregated away the Cas9-gRNA T-DNA insertion cassette.

All 5 alleles carried deletions in the *ZmWUS1-B* enhancer region. In particular, the *Bif3-Δ113* allele not only removed 2 AGATAT-binding motifs but also most of the duplicated 69 bp conserved sequence, while the *Bif3-Δ33* allele retained the 69 bp conserved sequence but removed the AGATAT-binding motif closest to the *ZmWUS1* proximal promoter. The remaining 3 smaller deletion alleles preserved all AGATAT-binding motifs but removed DNA sequence

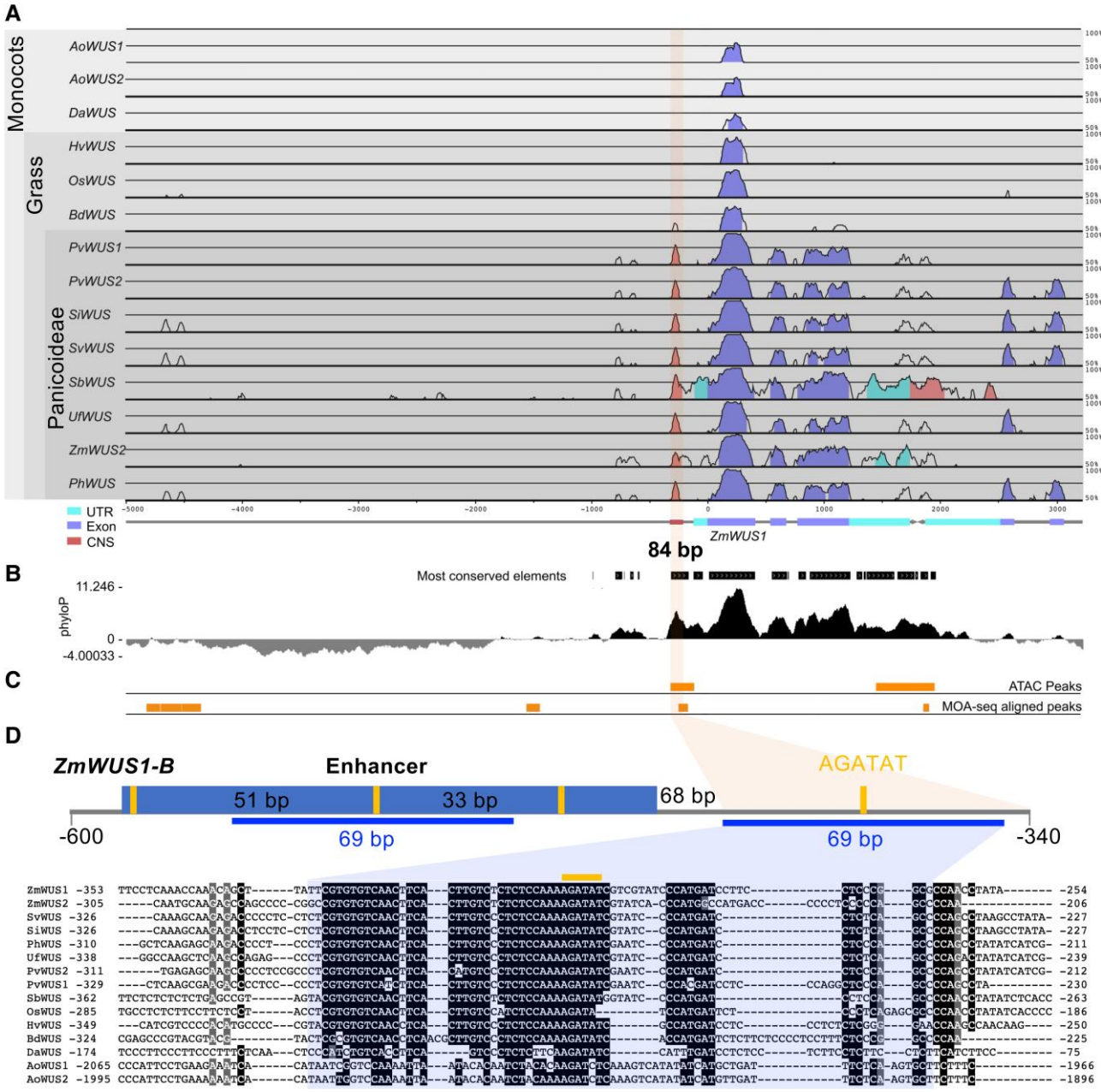

Figure 1. The *ZmWUS1* proximal promoter contains a conserved noncoding sequence in grasses. **A** and **B)** The proximal promoter of *ZmWUS1* contains an 84 bp noncoding sequence that is highly conserved across the Panicoideae (**A**, mVISTA analysis; **B**, phyloP analysis). UTR, untranslated region; CNS, conserved noncoding sequence. **C)** In maize, this conserved noncoding sequence is located in an open chromatin region (ATAC-seq (Hufford et al. 2021) and MOA-seq (Savadel et al. 2021)). **D)** Sequence annotation of the proximal region of the *ZmWUS1-B* promoter (−340 to −600 bp upstream of the start codon ATG). A 69 bp DNA fragment (blue line) within the 84 bp CNS has been duplicated and is present in both the proximal promoter and the *ZmWUS1-B* enhancer in *Bif3* mutants. Denim box, enhancer DNA; orange lines, AGATAT-binding motifs. The 51, 33, and 68 bp indicate the respective distances between 2 adjacent AGATAT-binding motifs. Numbers next to the aligned sequences indicate distance from the start codon. *Ao*, *Asparagus officinalis*; *Da*, *Dioscorea alata*; *Hv*, *Hordeum vulgare*; *Os*, *Oryza sativa*; *Bd*, *Brachypodium distachyon*; *Pv*, *Panicum virgatum*; *Si*, *Setaria italica*; *Sv*, *Setaria viridis*; *Sb*, *Sorghum bicolor*; *Uf*, *Urochloa fusca*; *Ph*, *Panicum hallii*.

between the first AGATAT-binding motif and the junction site (Supplemental Fig. S2); we therefore only focused on the *Bif3* -Δ*15* allele that encompasses the deleted sequences of both *Bif3*-Δ*4* and *Bif3*-Δ*1* alleles (Fig. 2B, Supplemental Fig. S2). As *Bif3* mutants in A619 showed a unique ball-shaped ear phenotype (Chen et al. 2021), we asked whether these new alleles also affected the *Bif3* phenotype. Plants carrying the heterozygous *Bif3*-Δ*113* or *Bif3*-Δ*33* alleles consistently showed a normal ear phenotype, indistinguishable from WT siblings. However, plants carrying the heterozygous *Bif3*-Δ*15* allele failed to complement the *Bif3* ear phenotype and instead consistently showed ball-shaped ears (Fig. 2B). As *Bif3*

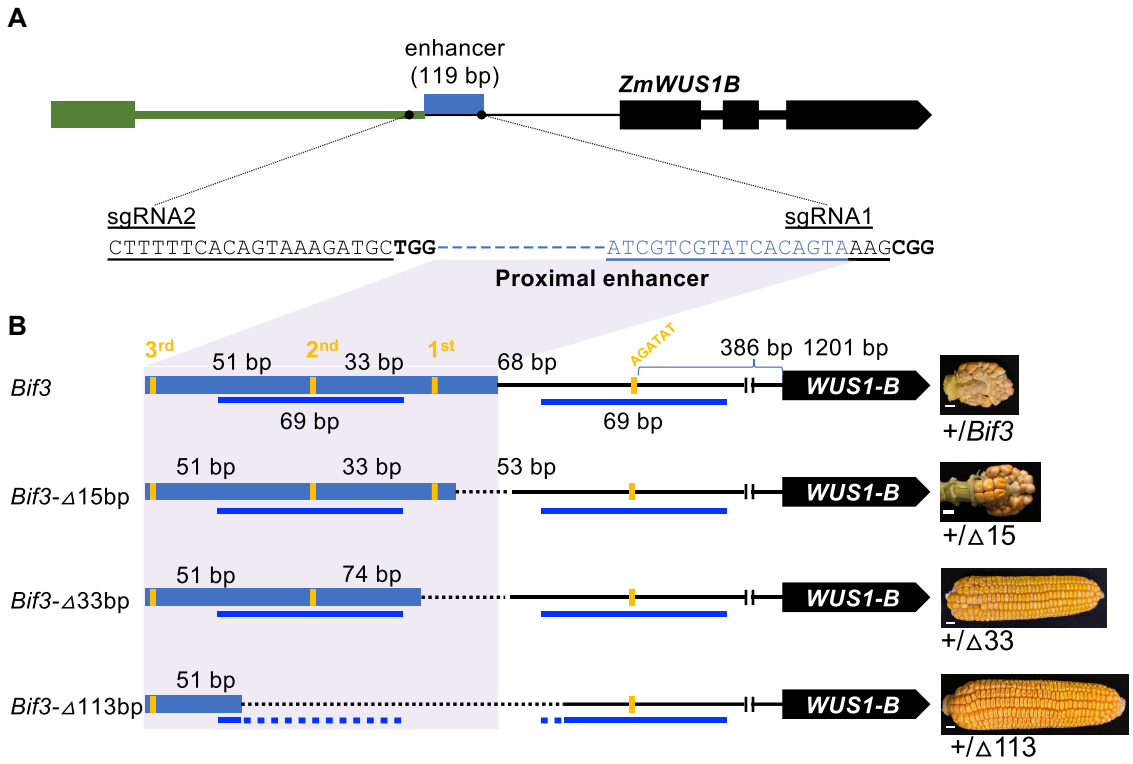

Figure 2. CRISPR-Cas9 editing of the *ZmWUS1-B* enhancer. **A)** Two sgRNAs were designed to target the enhancer of *ZmWUS1-B*. Black dots, sgRNAs; denim box, proximal enhancer of *ZmWUS1-B*; other colored boxes, exons; colored thick lines, introns. **B)** Three edited alleles of the *ZmWUS1-B* enhancer region and their corresponding phenotypic effects. The distances between 2 adjacent AGATAT are shown. Blue lines, 69 bp CNS; dashed lines, deletions by CRISPR-Cas9. Scale bars in **B)**, 1 cm.

mutants had disorganized inflorescence meristems and barren patches in inflorescences, we used scanning electron microscopy (SEM) to analyze 4 to 5 mm developing ear primordia of the edited alleles. Both heterozygous *Bif3-Δ113* and *Bif3-Δ33* alleles showed normal ear primordium development relative to those of the control siblings, while the *Bif3-Δ15* allele showed disorganized inflorescence meristems, similar to the original *Bif3* mutant ears (Fig. 3A (Chen et al. 2021)). These results suggest that duplication of the 69 bp conserved region in the *ZmWUS1-B* enhancer region is not a major driver of developmental defects in *Bif3* mutant ears but rather that meristem defects result from the presence of 4 AGATAT motifs controlling *ZmWUS1-B* expression.

We next asked to what degree editing of the *ZmWUS1-B* enhancer region influenced *ZmWUS1* expression by measuring transcript levels in 3 to 5 mm developing ear primordia using RT-qPCR. Heterozygous *Bif3-Δ113*, *Bif3-Δ33*, and *Bif3-Δ15* mutants showed elevated expression levels of 1.6× ($P < 0.01$), 1.9× ($P < 0.01$), and 2.3× ($P < 0.0001$) in comparison with their corresponding control siblings, respectively (Fig. 3B). In addition, we examined the ear phenotype of the homozygous *Bif3-Δ113* and *Bif3-Δ33* alleles. We found that the homozygous *Bif3-Δ113* allele appeared similar to WT, while the homozygous *Bif3-Δ33* allele exhibited an obvious *Bif3* ear phenotype (Fig. 3, C and D). These data indicate that there is an expression threshold of *ZmWUS1* in affecting inflorescence meristem function.

To further evaluate the effect of the different edited alleles on the activity of the *ZmWUS1* proximal promoter (444 bp DNA upstream of ATG, named pWUS1; (Chen et al. 2021)), we performed transactivation dual-luciferase assays in maize protoplasts by cloning each enhancer allele (*Bif3-Δ113*, *Bif3-Δ33*, and *Bif3-Δ15*) along with the *ZmWUS1* proximal promoter and using them to drive firefly luciferase expression. In the presence of overexpressed *ZmRR8*, the *Bif3-Δ113*, *Bif3-Δ33*, and *Bif3-Δ15* promoter alleles showed a 1.6×, 2.3×, and 3.03× respective increase ($P < 0.05$) relative to the 444 bp proximal promoter of *ZmWUS1*; similarly, overexpressed *ZmRR11* showed a 1.6×, 2.5×, and 3.5× respective increase ($P < 0.001$) (Fig. 3, E and F). These results suggest that increasing numbers of type B RR binding motifs result in a linear and additive effect on *ZmWUS1* levels of transcription.

Type B RRs are known to homo- and heterodimerize (Veerabagu et al. 2012; Djeghdir et al. 2021) possibly allowing them to work cooperatively to bind adjacent sites. We therefore analyzed our edited *ZmWUS1-B* alleles and noted that they showed altered spacing distances among AGATAT core motifs (Fig. 2B). Furthermore, the allelic series (Fig. 2B) highlighted the importance of the first motif in the *ZmWUS1-B* enhancer region: the *Bif3-Δ33* and *Bif3-Δ15* mutants showed very different ear phenotypes but carried only minor sequence differences. These observations prompted us to examine the effect of the intermotif spacing between the first 2 AGATAT motifs on

enhancer functionality. To this end, we generated 2 additional enhancer variants by removing 22 bp of DNA from the 33 bp spacing sequence that separated the first and second AGATAT motifs, resulting in a spacing of 11 bp between 2 AGATAT motifs (S11), and by inserting 10 bp (TTTTTA AAAT; S43) into the same spacing sequence, leading to a 43 bp distance between the 2 elements (Fig. 3E; Supplemental Fig. S3). Next, we compared the effects of these enhancer variants on the *ZmWUS1* proximal promoter activity with the original *ZmWUS1-B* p570 promoter (Supplemental Fig. S3 (Chen et al. 2021)). Using transactivation dual-luciferase assays in maize protoplasts with overexpressed *ZmRR8* or *ZmRR11*, we found that there were no statistical significant differences among all 3 promoter regions tested (Fig. 3, E and G). These findings indicate that the intermotif spacing of type B RR binding motifs does not have a substantial impact on expression. While the 18 bp difference between the *Bif3-Δ33* and *Bif3-Δ15* alleles may encompass additional TF binding sites (TFBSs), previous data indicated that the increased expression of *ZmWUS1-B* is due to the 3 additional AGATAT motifs (Chen et al. 2021). Overall, we conclude that the *ZmWUS1-B* enhancer activity is due to the additive effect of individual AGATAT type B RR binding motifs.

The *ZmWUS1* gene, which positively regulates the stem cell population in inflorescence meristems, was found to be slightly overexpressed in both heterozygous *Bif3-Δ113* and *Bif3-Δ33* alleles (Fig. 3B). We hypothesized that these alleles, while consistently exhibiting a normal ear phenotype, may still be able to increase inflorescence meristem size and ultimately the number of kernel rows. We therefore scored additional traits in families that segregated for edited or WT alleles. At the 5 mm stage, only developing ear primordia of heterozygous *Bif3-Δ33* alleles showed slightly enlarged inflorescence meristems (Fig. 4A), corresponding to the higher expression level of *ZmWUS1* during this developmental stage (Fig. 3B). However, the kernel row number of heterozygous *Bif3-Δ33* plants (and *Bif3-Δ113* plants) was not affected when compared with control siblings (Fig. 4B). Surprisingly, we instead observed increased prolificacy in the *Bif3-Δ33* allele, with an average of 2 ears produced in the primary lateral branches compared with 1 ear in the primary lateral branches of control siblings (Fig. 4, C and D), suggesting that increasing *ZmWUS1* expression might have pleiotropic effects in inflorescence architecture yet to be investigated.

There are currently 3 predominant models to explain the distinct ways enhancers and TFs interact to form active regulatory regions: the billboard, enhanceosome, and TF collective models (Jindal and Farley 2021; Schmitz et al. 2022). In the billboard model, CREs located near each other form a *cis*-regulatory module (CRM); yet, each CRE can still have a unique impact on gene expression. The enhancer serves as a unit of information, with the elements arranged for interpretation by the basic transcriptional machinery and whose elements can be rearranged without affecting its overall function (Spitz and Furlong 2012). In the enhanceosome model, enhancer DNA sequence is highly structured and requires precise arrangement of TFBSs to facilitate functional binding of TFs and transcriptional activation (Jindal and Farley 2021). In the TF collective model instead, enhancers are occupied by a group of TFs through a combination of TF binding and physical interactions between TFs (Jindal and Farley 2021). Based on our in vivo analysis of the 119 bp *ZmWUS1-B* enhancer, additional AGATAT motifs have an additive impact on the activity of the *ZmWUS1-B* promoter. This is mostly consistent with a billboard model whereby having extra AGATAT motifs locally increases the concentration of type B RR proteins resulting in enhanced transcriptional activation. The examination of 5 different enhancer edits (3 deletions, 1 insertion, and 1 deletion altering intermotif spacing) showed that the DNA rearrangement does not compromise the overall function of individual AGATAT CREs.

Our results also show that in maize inflorescence meristems, *ZmWUS1* can be upregulated up to 2.5-fold (approximately) without notably impacting ear development, presumably as a result of the buffering that is afforded by the CLV-WUS negative feedback loop (Nimchuk et al. 2015; Liu et al. 2021; Plong et al. 2021; Schlegel et al. 2021). *ZmCLE7*, one of the *CLV3* maize homologs, was reportedly upregulated up to 8-fold in the inflorescences of the dominant *Bif3* mutant, suggesting that *ZmWUS1* may directly regulate *ZmCLE7* expression and that both are integral to the feedback mechanism (Chen et al. 2021). This pathway appears more sensitive than the buffering of *CLV3* fluctuations in the *Arabidopsis* shoot apical meristem (Müller et al. 2006) and may be also influenced by the presence of the paralogous gene *ZmWUS2* (Nardmann and Werr 2006) which is downregulated in *Bif3* ears (Chen et al. 2021), possibly as a compensatory mechanism.

Multimerization of type B RR binding sites represents the basis of the widely used cytokinin signaling reporter *TCS* (Müller and Sheen 2008). In a recently improved version called *TCSv2*, a different arrangement of type B ARR binding sites results in increased sensitivity of the reporter (Steiner et al. 2020). In maize, a *TCS* reporter line was generated based on the Arabidopsis *TCSv2* reporter, containing multimerized 5′-(A/G)GAT(T/C)-3′ motifs (Steiner et al. 2020; Robil and McSteen 2023). Our results suggest that multimerization of the AGATAT motif (a slightly different motif relative to TCSv2) found in the *Bif3* locus could be used to design an improved marker for monitoring cytokinin response in grass meristems. In summary, we showed that *ZmWUS1* expression can be precisely controlled by the number of individual AGATAT motifs in its proximal promoter region. Understanding the fine tuning of *WUS* gene expression in the context of meristem development and regulation is particularly relevant to morphogenic-based crop transformation technologies (Gordon-Kamm et al. 2019). Given that the AGATAT motifs are located within an evolutionarily conserved region, the type B RR-AGATAT interaction represents a conserved module to activate *WUS* expression and could be engineered to provide a controlled increase of expression levels of *WUS* genes in different species.

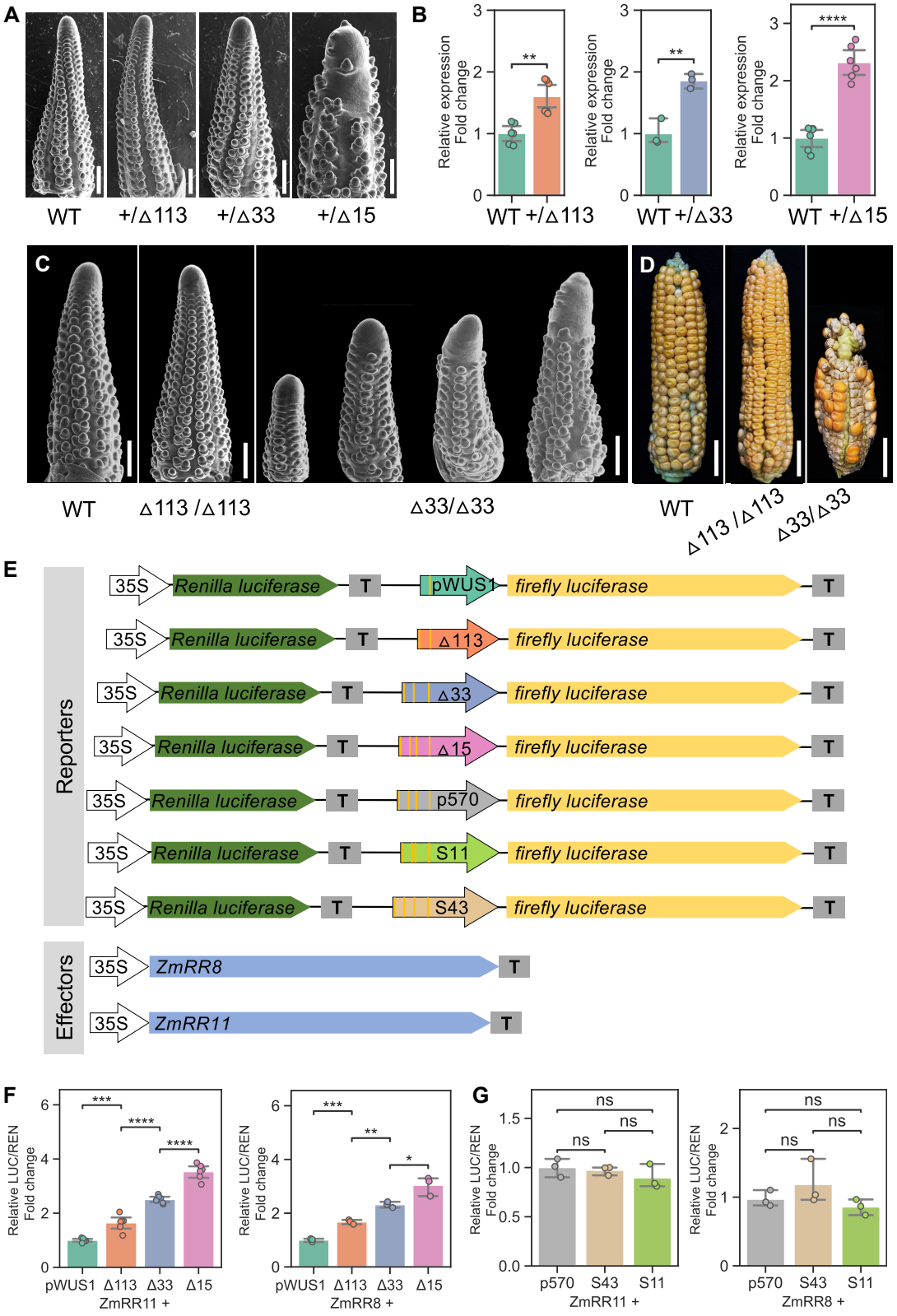

Figure 3. Type B RRs binding sites show additive effect on the expression of *ZmWUS1-B*. **A)** SEM images of WT and edited ear primordia. WT, wild-type siblings; +/△*113*, heterozygous 113 bp deletion at the enhancer region; +/△33, heterozygous 33 bp deletion at the enhancer region; +/△*15*, heterozygous 15 bp deletion at the enhancer region. Scale bars 500 μm. **B)** RT-qPCR assays comparing *ZmWUS1* expression in 3 enhancer-edited mutants. For each genotype, a minimum of 3 biological replicates were performed. **C)** SEMs of immature ears of WT and homozygous △*113* and △33

(continued)

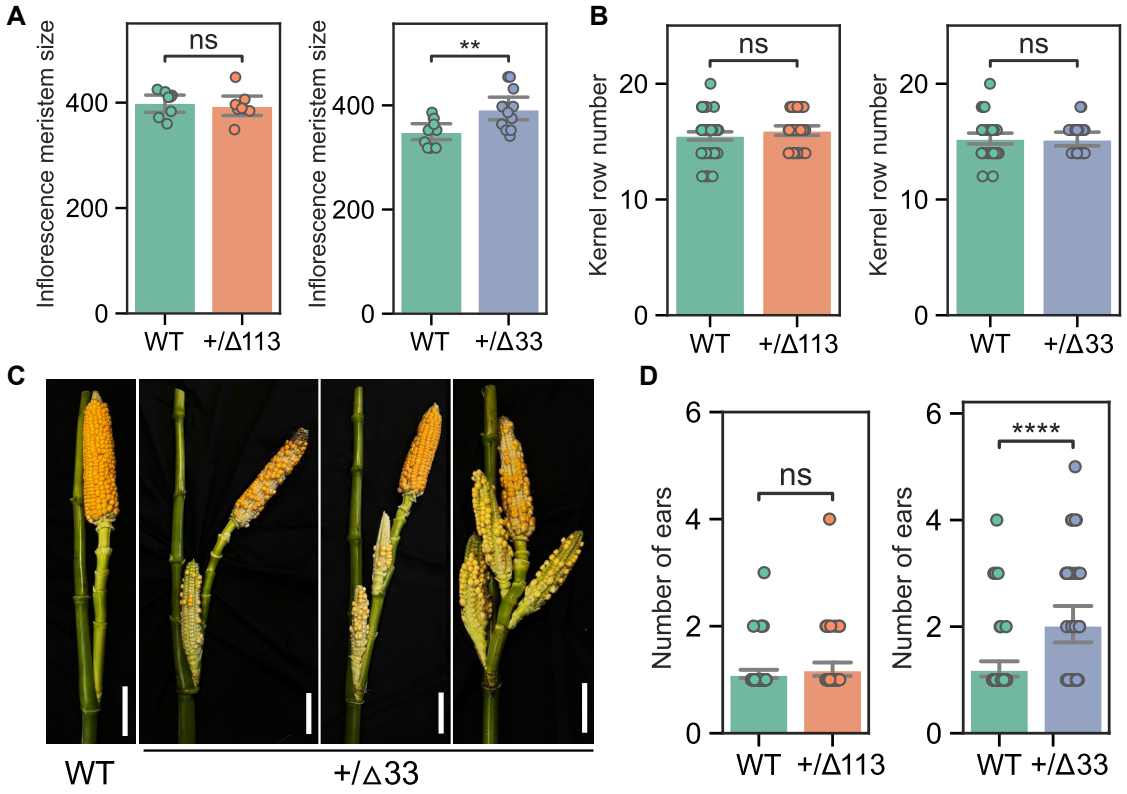

Figure 4. *ZmWUS1-B*-edited alleles do not increase kernel row number but enhance maize prolificacy. **A** and **B)** Comparison of inflorescence meristem size (in μm; *y* axis) and kernel row number of WT and heterozygous *Δ113* and *Δ33* alleles. For the quantification of inflorescence meristem sizes, $n = 8$ in +/*Δ113* plants and WT siblings; $n = 12$ in +/*Δ33* plants, and $n = 10$ in WT siblings. For the quantification of kernel row number, $n = 43$ in +/*Δ113* allele plants and 65 in WT siblings, 28 in +/*Δ33* allele plants, and 44 in WT siblings. **C)** The heterozygous *Δ33* allele showed increased prolificacy. Scale bars 10 cm. **D)** Quantification of ear numbers of the primary lateral branches in heterozygous *Δ113* and *Δ33* alleles. $n = 56$ in +/*Δ113* allele plants and 65 in WT siblings, 44 in +/*Δ33* allele plants, and 63 in WT siblings. Student's *t* tests *P*-value annotation legend: ns, $P > 0.05$; **$0.001 < P < 0.01$; ****$P < 0.0001$; error bars indicate 95% confidence interval.

Materials and methods

Genomic editing of *ZmWUS1-B* enhancer by CRISPR-Cas9

CRISPR-Cas9 was used to create mutations in the previously identified enhancer region of *ZmWUS1-B* (Chen et al. 2021). Two sgRNAs were designed based on the *Bif3* mutant sequence using CRISPOR (Concordet and Haeussler 2018). Both reverse complementary single-stranded guide DNAs (gDNAs) were synthesized and annealed to form double-stranded gDNAs with overhangs of GGCG at forward strands and AAAC at reversed strands. Two double-stranded gDNAs were cloned into a pENTR-OsU3p-scaffold by Golden Gate Assembly cloning. The gRNA array of OsU3p-gRNA1-scaffold and OsU3p-gRNA2-scaffold was assembled into the pBUE411 vector (Xing et al. 2014) using the Gibson Assembly Master Mix (New England Biolabs), and the resulting construct was transformed into maize (*Z. mays*) inbred line B104 via *A. tumefaciens*–mediated transformation. Transformation was carried out by the Iowa State Plant Transformation Facility. Genomic edits were screened by PCR amplification and Sanger sequencing of the target region. The resulting enhancer-edited alleles were backcrossed to A619 for 3 generations to remove the T-DNA insertion as well as to purify the genetic background before phenotypic and expression analysis. The guide RNA sequences for *ZmWUS1-B* enhancer and primers for gRNA array assembly

Figure 3. (Continued)
edits. SEM images were digitally extracted for comparison. Scale bars 500 μm. **D)** Mature ears of WT and homozygous *Δ113* and *Δ33* edits. Scale bars 2 cm. **E** to **G)** Transient transactivation in maize protoplasts. **E)** Reporter and effector constructs used in this study. The firefly luciferase is driven by the proximal promoter of *ZmWUS1-B* (denim arrows), including 444 bp (pWUS1), 570 bp of the *Bif3* allele (p570), and 3 CRISPR-edited *Bif3* alleles of *ZmWUS1-B* (*Δ113*, *Δ33*, and *Δ15*). Two additional promoters were synthesized to carry a deletion of 22bp (between the 1st and 2nd AGATAT motifs; S11) and an insertion of 10 bp (between the 1st and 2nd AGATAT motifs; S43). The Renilla luciferase driven by the CaMV 35S promoter is used for normalization. **F** and **G)** Quantification of promoter activities when induced by type B RRs, ZmRR8 and ZmRR11. A minimum of 3 biological replicates were performed. Student's *t* tests *P*-value annotation legend: ns, $P > 0.05$; *$0.01 < P < 0.05$; **$0.001 < P < 0.01$; ***$0.0001 < P < 0.001$; ****$P < 0.0001$; error bars indicate 95% confidence interval.

and enhancer-edited allele genotyping are listed in Supplemental Table S1.

Plant phenotyping

Images of inflorescence meristems were captured by SEM. For SEMs, fresh ear primordia (3 to 5 mm) were dissected and analyzed using a JMC-6000PLUS benchtop SEM (JEOL).

Expression analysis

RT-qPCR analysis was performed using an Illumina Eco Real-Time PCR System. At least 9 ear primordia were pooled for each genotype, and 3 biological replicates were performed for each assay. Total mRNA was extracted using RNeasy Mini Kit (Qiagen) with on-column DNase I (Qiagen) treatment and used for complementary DNA (cDNA) synthesis with a qScript cDNA synthesis kit (Quanta BioSciences). RT-qPCR was performed using gene-specific primers and the PerfeCTa SYBR Green FastMix (Quanta BioSciences). Target cycle threshold values were normalized using *ZmUBIQUITIN*. Primers used are listed in Supplemental Table S1.

Transactivation assays

Transactivation assays were conducted in maize mesophyll protoplasts as described previously (Chen et al. 2021). The effector vector pEarlyGate 100 was used for expression of *ZmRR8* and *ZmRR11* driven by the cauliflower mosaic virus (CaMV) dual 35S promoter. The reporter vector pGreenII 0800-LUC was used for detecting the transactivation activities of ZmRR8 and ZmRR11 on the original *ZmWUS1-B* promoter with a 119 bp insertion (p570), the *ZmWUS1-B* promoter without the 119 bp insertion (p444), and the 3 enhancer-edited promoters (*Bif3*-Δ*113*, *Bif3*-Δ33, and *Bif3*-Δ*15*). Two additional mutated enhancers with 11 bp and 43 bp spacing between the first 2 adjacent AGATAT-binding motifs were created by Golden Gate Assembly. Equal amounts of effector plasmids and reporter plasmids were cotransformed into mesophyll protoplasts of maize by PEG-mediated protoplast transformation. The protoplasts were incubated in the dark at 23 °C for 16 h for firefly luciferase/Renilla luciferase (LUC/REN) activity analysis. The ratio of LUC/REN activity was measured using the Dual-Luciferase Reporter Assay System (Promega). Primers used to amplify the *ZmWUS1-B* promoter with various enhancer edits are listed in Supplemental Table S1.

Evolutionary analysis

Orthologs of *ZmWUS1* and its paralog *ZmWUS2* and their corresponding 5 kb upstream and 2 kb downstream sequences were retrieved from Phytozome (https://phytozome-next.jgi.doe.gov/). Conserved regions were called using mVISTA with default settings (70% similarity and minimum size of 50 bp) (Frazer et al. 2004). The same regions were aligned via MAFFT (Katoh et al. 2002) and analyzed with phyloP from the PhastWeb (Ramani et al. 2019). The alignments of the *ZmWUS1* were analyzed with phyloP using the conservation–acceleration model to test for conservation and acceleration concurrently.

Statistics and reproducibility

Statistical significance was determined by 2-tailed Student's *t* tests; exact *P*-values of all comparisons are listed in Supplemental Table S2. All experiments have been replicated at least 3 times with similar or identical results, and/or data have been extracted using multiple biological samples. For SEMs, at least 3 independent samples were imaged with similar results; representative SEMs of the different genotypes analyzed are presented in the figures.

Accession numbers

ZmWUS1 corresponds to Zm00001eb067310 (B73v5). The *Bif3 ZmWUS1-B* sequence can be found in NCBI GenBank, accession MW677562.

Acknowledgments

The authors wish to thank Mary Galli for suggestions and critical reading of the manuscript and Themios (Tim) Chionis and John Bombardiere for greenhouse and field management.

Author contributions

Z.C. and A.G. conceived this study and designed all experiments; Z.C. and L.C. performed experiments and collected data; Z.C. and A.G. wrote the manuscript; A.G. obtained funding and is responsible for this manuscript. All authors read and approved the manuscript.

Supplementary data

The following materials are available in the online version of this article.

Supplemental Figure S1. The AGATAT-binding motifs of *WUS* genes are conserved in eudicot species.

Supplemental Figure S2. Mutation in the ZmWUS1-B enhancer by CRISPR-Cas9.

Supplemental Figure S3. Engineered enhancer variants with different distances between 2 AGATAT-binding motifs.

Supplemental Table S1. Primers used in this study.

Supplemental Table S2. Exact *P*-values.

Funding

This work was supported by grants from the National Science Foundation (IOS#2026561 and IOS#1916804). L.C., an undergraduate student from CUNY Brooklyn College, was supported by the Research Intensive Summer Experience (RISE) program at Rutgers University.

Conflict of interest statement. None declared.

Data availability

The data underlying this article will be shared on reasonable request to the corresponding author.

References

Chen ZL, Li W, Gaines C, Buck A, Galli M, Gallavotti A. Structural variation at the maize WUSCHEL1 locus alters stem cell organization in inflorescences. Nat Commun. 2021:**12**(1):2378. https://doi.org/10.1038/s41467-021-22699-8

Concordet JP, Haeussler M. CRISPOR: intuitive guide selection for CRISPR/Cas9 genome editing experiments and screens. Nucleic Acids Res. 2018:**46**(W1):W242–W245. https://doi.org/10.1093/nar/gky354

Djeghdir I, Chefdor F, Bertheau L, Koudounas K, Carqueijeiro I, Cruz PL, Courdavault V, Depierreux C, Larcher M, Lamblin F, et al. Evaluation of type-B RR dimerization in poplar: a mechanism to preserve signaling specificity? Plant Sci. 2021:**313**:111068. https://doi.org/10.1016/j.plantsci.2021.111068

Frazer KA, Pachter L, Poliakov A, Rubin EM, Dubchak I. VISTA: computational tools for comparative genomics. Nucleic Acids Res. 2004:**32**(Web Server):W273–W279. https://doi.org/10.1093/nar/gkh458

Gordon-Kamm B, Sardesai N, Arling M, Lowe K, Hoerster G, Betts S, Jones T. Using morphogenic genes to improve recovery and regeneration of transgenic plants. Plants (Basel). 2019:**8**(2):38. https://doi.org/10.3390/plants8020038

Hufford MB, Seetharam AS, Woodhouse MR, Chougule KM, Ou SJ, Liu JN, Ricci WA, Guo TT, Olson A, Qiu YJ, et al. De novo assembly, annotation, and comparative analysis of 26 diverse maize genomes. Science 2021:**373**(6555):655–662. https://doi.org/10.1126/science.abg5289

Ikeda M, Mitsuda N, Ohme-Takagi M. Arabidopsis WUSCHEL is a bifunctional transcription factor that acts as a repressor in stem cell regulation and as an activator in floral patterning. Plant Cell. 2009:**21**(11):3493–3505. https://doi.org/10.1105/tpc.109.069997

Jindal GA, Farley EK. Enhancer grammar in development, evolution, and disease: dependencies and interplay. Dev Cell. 2021:**56**(5):575–587. https://doi.org/10.1016/j.devcel.2021.02.016

Katoh K, Misawa K, Kuma K, Miyata T. MAFFT: a novel method for rapid multiple sequence alignment based on fast Fourier transform. Nucleic Acids Res. 2002:**30**(14):3059–3066. https://doi.org/10.1093/nar/gkf436

Kitagawa M, Jackson D. Control of meristem size. Annu Rev Plant Biol. 2019:**70**(1):269–291. https://doi.org/10.1146/annurev-arplant-042817-040549

Liu L, Gallagher J, Arevalo ED, Chen R, Skopelitis T, Wu QY, Bartlett M, Jackson D. Enhancing grain-yield-related traits by CRISPR-Cas9 promoter editing of maize CLE genes. Nat Plants. 2021:**7**(3):287–294. https://doi.org/10.1038/s41477-021-00858-5

Müller B, Sheen J. Cytokinin and auxin interaction in root stem-cell specification during early embryogenesis. Nature 2008:**453**(7198):1094–1097. https://doi.org/10.1038/nature06943

Müller R, Borghi L, Kwiatkowska D, Laufs P, Simon R. Dynamic and compensatory responses of Arabidopsis shoot and floral meristems to CLV3 signaling. Plant Cell. 2006:**18**(5):1188–1198. https://doi.org/10.1105/tpc.105.040444

Nardmann J, Werr W. The shoot stem cell niche in angiosperms: expression patterns of WUS orthologues in rice and maize imply major modifications in the course of mono- and dicot evolution. Mol Biol Evol. 2006:**23**(12):2492–2504. https://doi.org/10.1093/molbev/msl125

Nimchuk ZL, Zhou Y, Tarr PT, Peterson BA, Meyerowitz EM. Plant stem cell maintenance by transcriptional cross-regulation of related receptor kinases. Development 2015:**142**(6):1043–1049. https://doi.org/10.1242/dev.119677

Perales M, Rodriguez K, Snipes S, Yadav RK, Diaz-Mendoza M, Reddy GV. Threshold-dependent transcriptional discrimination underlies stem cell homeostasis. Proc Natl Acad Sci USA. 2016:**113**(41):E6298–E6306. https://doi.org/10.1073/pnas.1607669113

Plong A, Rodriguez K, Alber M, Chen WT, Reddy GV. CLAVATA3 mediated simultaneous control of transcriptional and post-translational processes provides robustness to the WUSCHEL gradient. Nat Commun. 2021:**12**(1):6361. https://doi.org/10.1038/s41467-021-26586-0

Ramani R, Krumholz K, Huang YF, Siepel A. PhastWeb: a web interface for evolutionary conservation scoring of multiple sequence alignments using phastCons and phyloP. Bioinformatics. 2019:**35**(13):2320–2322. https://doi.org/10.1093/bioinformatics/bty966

Robil JM, McSteen P. Hormonal control of medial-lateral growth and vein formation in the maize leaf. New Phytol. 2023:**238**(1):125–141. https://doi.org/10.1111/nph.18625

Savadel SD, Hartwig T, Turpin ZM, Vera DL, Lung PY, Sui X, Blank M, Frommer WB, Dennis JH, Zhang JF, et al. The native cistrome and sequence motif families of the maize ear. PLoS Genet. 2021:**17**(8):e1009689. https://doi.org/10.1371/journal.pgen.1009689

Schlegel J, Denay G, Wink R, Pinto KG, Stahl Y, Schmid J, Blümke P, Simon RGW. Control of Arabidopsis shoot stem cell homeostasis by two antagonistic CLE peptide signalling pathways. eLife 2021:**10**:e70934. https://doi.org/10.7554/eLife.70934

Schmitz RJ, Grotewold E, Stam M. Cis-regulatory sequences in plants: their importance, discovery, and future challenges. Plant Cell. 2022:**34**(2):718–741. https://doi.org/10.1093/plcell/koab281

Spitz F, Furlong EEM. Transcription factors: from enhancer binding to developmental control. Nat Rev Genet. 2012:**13**(9):613–626. https://doi.org/10.1038/nrg3207

Steiner E, Israeli A, Gupta R, Shwartz I, Nir I, Leibman-Markus M, Tal L, Farber M, Amsalem Z, Ori N, et al. Characterization of the cytokinin sensor TCSv2 in arabidopsis and tomato. Plant Methods 2020:**16**(1):152. https://doi.org/10.1186/s13007-020-00694-2

Veerabagu M, Elgass K, Kirchler T, Huppenberger P, Harter K, Chaban C, Mira-Rodado V. The Arabidopsis B-type response regulator 18 homomerizes and positively regulates cytokinin responses. Plant J. 2012:**72**(5):721–731. https://doi.org/10.1111/j.1365-313X.2012.05101.x

Wang XG, Aguirre L, Rodriguez-Leal D, Hendelman A, Benoit M, Lippman ZB. Dissecting cis-regulatory control of quantitative trait variation in a plant stem cell circuit. Nat Plants. 2021:**7**(4):419–427. https://doi.org/10.1038/s41477-021-00898-x

Xie MT, Chen HY, Huang L, O'Neil RC, Shokhirev MN, Ecker JR. A B-ARR-mediated cytokinin transcriptional network directs hormone cross-regulation and shoot development. Nat Commun. 2018:**9**(1):1604. https://doi.org/10.1038/s41467-018-03921-6

Xing HL, Dong L, Wang ZP, Zhang HY, Han CY, Liu B, Wang XC, Chen QJ. A CRISPR/Cas9 toolkit for multiplex genome editing in plants. BMC Plant Biol. 2014:**14**(1):327. https://doi.org/10.1186/s12870-014-0327-y

Zhang TQ, Lian H, Zhou CM, Xu L, Jiao YL, Wang JW. A two-step model for de novo activation of WUSCHEL during plant shoot regeneration. Plant Cell. 2017:**29**(5):1073–1087. https://doi.org/10.1105/tpc.16.00863

Zubo YO, Blakley IC, Yamburenko MV, Worthen JM, Street IH, Franco-Zorrilla JM, Zhang WJ, Hill K, Raines T, Solano R, et al. Cytokinin induces genome-wide binding of the type-B response regulator ARR10 to regulate growth and development in Arabidopsis. Proc Natl Acad Sci USA. 2017:**114**(29):E5995–E6004. https://doi.org/10.1073/pnas.1620749114